Available online at www.sciencedirect.com
SCIENCE DIRECT®
Physica A 318 (2003) 319–333
PHYSICA A
www.elsevier.com/locate/physa

Quantitative comparison of mean field mixing laws for conductivity and dielectric constants of porous media

J. Widjajakusuma[a,*], B. Biswal[a,b], R. Hilfer[a,c]

[a] *ICA-1, Universität Stuttgart, Pfaffenwaldring 27, 70569 Stuttgart, Germany*
[b] *Department of Physics, Sri Venkateswara College, New Delhi 110 021, India*
[c] *Institut für Physik, Universität Mainz, 55099 Mainz, Germany*

Received 4 June 2002

Abstract

Exact numerical solution of the electrostatic disordered potential problem is carried out for four fully discretized three-dimensional experimental reconstructions of sedimentary rocks. The measured effective macroscopic dielectric constants and electrical conductivities are compared with parameter-free predictions from several mean field type theories. All these theories give agreeable results for low contrast between the media. Predictions from local porosity theory, however, match for the entire range of contrast.

PACS: 61.43.Gt; 72.80.−r; 72.80.Tm; 78.55.Mb; 81.05.Rm

Keywords: Porous media; Conductivity; Transport

1. Introduction

Quantitative and parameter-free prediction of effective macroscopic transport parameters for composites, porous media, alloys and other heterogeneous mixtures is a recurrent unsolved problem of great importance [1,18]. Physical and technological applications range from hydrocarbon production through catalysis to polymer research. Some recent works on this problem are the prediction of permeability of fibre webs

* Corresponding author.

0378-4371/03/$ - see front matter
PII: S0378-4371(02)01197-4

[2], electrical conductivity of porous media [3–5], optical properties of gold deposits [6], dielectric spectroscopy of confined polar materials [7] and silica glasses [8], the conductivity of composite materials [9], or diffusion in catalysts [10].

Such macroscopic transport coefficients of two-phase mixtures depend crucially on the properties of the two constituents and the underlying microstructure. Quantitative prediction is difficult due to the great variety of different microstructures. Many unsuccessful attempts have been made to identify those geometric properties of the microstructure that correlate strongly with the physical transport coefficients. Simple mean field type theories [11–14] and variational bounds [15,16] correlate the transport properties with one-point correlation function, i.e., porosity or volume fraction. More advanced theories include information about higher-point correlations in the microstructure [17]. Local Porosity Theory (LPT) [1,3,18] includes distributions of local geometric observables from integral geometry [18–20]. Basic observables such as porosity, specific surface, connectivity and curvature measures (see [20,21]) are evaluated locally in LPT [1,3,18]. Classical mixing-laws, such as Bruggeman's effective medium equation or Clausius–Mossotti approximation can be shown to be special cases of LPT [1].

In this work we test the predictions of LPT for the electrical conductivity and dielectric constant through a comprehensive comparison with predictions from many existing mean field type theories and exact results obtained from numerical solution of the disordered potential problem. The paper is organized as follows: Section 2 summarises the geometric characterization of porous media in LPT and Section 3 summarises the effective material parameters measured numerically. In Section 4 we discuss some of the existing classical mixture formulae [1,22,23] and present a short derivation of the mixing-law based on LPT. In Section 5 we discuss some of the relevant length scales in LPT. The finite volume method [24,25] used to calculate the exact effective permittivities and conductivities of sandstones is presented in Section 6 and the LPT results are compared with those from classical mixture laws in the concluding Section 7.

2. Local geometric characteristic functions

We define $\mathbb{P} \subset \mathbb{S}$ in $\mathbb{R}^3$ to be the pore space of a biphasic porous medium $\mathbb{S}$. The matrix space $\mathbb{M}$ is the complement of $\mathbb{P}$ relative to $\mathbb{S}$. The sample $\mathbb{S}$ is discretized into a rectangular parallelepiped (simple cubic lattice) whose sidelengths are M_1, M_2 and M_3 in units of the lattice constant a (resolution of the discretization process). The total number of voxels in $\mathbb{S}$ is $N = M_1 M_2 M_3$.

The basic idea of LPT is to measure geometric observables such as porosity, specific internal surface or connectivity within a compact subset of the porous medium and to collect these measurements into various histograms [3,18]. Within a cubical measurement cell $\mathbb{K}(r, L)$ of sidelength L centered at the lattice vector $\mathbf{r}$, the local porosity is defined as

$$\phi(\mathbf{r}, L) = \frac{V(\mathbb{P} \cap \mathbb{K}(\mathbf{r}, L))}{V(\mathbb{K}(\mathbf{r}, L))}\,, \tag{1}$$

where $V(\mathbb{K}(\mathbf{r},L))$ denotes the volume of a subset $\mathbb{K} \subset \mathbb{R}^3$. The *local porosity distribution* $\mu(\phi,L)$ is given by

$$\mu(\phi,L) = \frac{1}{m}\sum_{\mathbf{r}} \delta(\phi - \phi(\mathbf{r},L)) \,, \tag{2}$$

where m is the number of placements of the measurement cell $\mathbb{K}(\mathbf{r},L)$ and $\delta(\phi-\phi(\mathbf{r},L))$ is the Dirac delta function. Ideally, all measurement cells should be disjoint. In small samples adequate statistics can be obtained by placing $\mathbb{K}(\mathbf{r},L)$ on all lattice sites $\mathbf{r}$ which are at least a distance $L/2$ from the boundary of $\mathbb{S}$, hence $m = \prod_{i=1}^{3}(M_i - L + 1)$. The support of the empirical probability density function (histogram) of local porosities $\mu(\phi,L)$ is the unit interval. The *average local porosity* $\bar{\phi}(L)$ is defined as

$$\bar{\phi}(L) = \int_0^1 \phi\mu(\phi,L)\,\mathrm{d}\phi \,. \tag{3}$$

For a homogeneous medium $\bar{\phi}(L)$ is independent of L. The bulk porosity $\phi(\mathbb{S})$ is the ratio of the volume of the pore space to the volume of the total sample, i.e., $\phi(\mathbb{S}) = V(\mathbb{P})/V(\mathbb{S})$.

The local connectivity properties of the porous medium are quantified as follows. A measurement cell $\mathbb{K}(\mathbf{r},L)$ is *percolating in the* x-(y-, z-)*direction* if there exists a connected path lying inside the pore space within the measurement cell between two points on the opposite boundary faces of $\mathbb{K}(\mathbf{r},L)$ perpendicular to the x-(y-, z-)axis. The indicator function for the connectivity of a cell is defined as

$$\Lambda(\mathbf{r},L) = \begin{cases} 1 & \text{if } \mathbb{K}(\mathbf{r},L) \text{ percolates in all three directions} \,, \\ 0 & \text{otherwise} \,. \end{cases} \tag{4}$$

The function $\Lambda(\mathbf{r},L)$ is measured using the Hoshen–Kopelman algorithm [26]. The *local percolation probability* $\lambda(\phi,L)$ is defined through

$$\lambda(\phi,L) = \frac{\sum_{\mathbf{r}} \Lambda(\mathbf{r},L)\delta_{\phi\phi(\mathbf{r},L)}}{\sum_{\mathbf{r}} \delta_{\phi\phi(\mathbf{r},L)}} \,. \tag{5}$$

It gives the fraction of measurement cells of sidelength L with local porosity ϕ that are percolating in all three directions. Here $\delta_{\phi\phi(\mathbf{r},L)}$ is the Kronecker delta. The *total fraction of percolating cells* of size L is given by integration over all local porosities,

$$p(L) = \int_0^1 \mu(\phi,L)\lambda(\phi,L)\,\mathrm{d}\phi \,. \tag{6}$$

The function $p(L)$ characterizes the overall connectivity of the sample at length scale L and is an important parameter for predicting the conductivity of porous media [1,21,27,28]. $\lim_{L\to\infty} p(L) = 0$ if $\mathbb{P}$ is disconnected while $\lim_{L\to\infty} p(L) = 1$ if $\mathbb{P}$ is globally connected. As $\lim_{L\to 0} \lambda(\phi,L) = \phi$, from Eq. (3) $\lim_{L\to 0} p(L) = \bar{\phi}$. Using this function, the microgeometries of some of these samples have been compared with

each other [29] and also with stochastic reconstruction models of Fontainebleau sandstone [30].

3. Electrostatic potential problem for disordered systems

In this work we restrict our attention to calculating the electrical permittivity and conductivity from a given microstructure. The mathematical formulation, however, is common to all problems of potential theory for disordered systems including thermal conduction, magnetostatics and diffusion [18].

The basic equations for the electric displacement vector $\mathbf{D}(\mathbf{r})$ and the electric field $\mathbf{E}(\mathbf{r})$ in electrostatics are

$$\nabla \cdot \mathbf{D}(\mathbf{r}) = 0; \quad \mathbf{E}(\mathbf{r}) = -\nabla U(\mathbf{r}), \quad \mathbf{D}(\mathbf{r}) = \varepsilon(\mathbf{r})\mathbf{E}(\mathbf{r}), \quad \mathbf{r} \in \mathbb{P}\,, \tag{7}$$

where $U(\mathbf{r})$ is the electric potential. These equations remain valid for $\mathbf{r} \in \mathbb{M} = \mathbb{S} - \mathbb{P}$. The position dependent permittivity $\varepsilon(\mathbf{r})$ (in units of ε_0, the dielectric permittivity of the vacuum) is given by

$$\varepsilon(\mathbf{r}) = \varepsilon_{\mathbb{P}}\chi_{\mathbb{P}}(\mathbf{r}) + \varepsilon_{\mathbb{M}}\chi_{\mathbb{M}}(\mathbf{r})\,, \tag{8}$$

where $\varepsilon_{\mathbb{P}}$ and $\varepsilon_{\mathbb{M}}$ are the (isotropic) permittivities of $\mathbb{P}$ and $\mathbb{M}$, respectively. The random microstructure is represented through the indicator function:

$$\chi_{\mathbb{G}}(\mathbf{r}) = \begin{cases} 1 & \text{for } \mathbf{r} \in \mathbb{G}\,, \\ 0 & \text{for } \mathbf{r} \notin \mathbb{G}\,. \end{cases} \tag{9}$$

The effective permittivity $\bar{\varepsilon}$ is obtained by ensemble averaging of Eq. (7)

$$\langle \mathbf{D}(\mathbf{r}) \rangle = \bar{\varepsilon} \langle \mathbf{E}(\mathbf{r}) \rangle\,. \tag{10}$$

The microheterogeneous medium is assumed to be stationary and ergodic, therefore the ensemble average of a field $\mathbf{f}(\mathbf{r})$ is equivalent to the volume average over the region $\mathbb{G}$.

$$\langle \mathbf{f}(\mathbf{r}) \rangle_{\mathbb{G}} = \frac{1}{V(\mathbb{G})} \int_{\mathbb{G}} \mathbf{f}(\mathbf{r})\, \mathrm{d}V\,. \tag{11}$$

Because the derivative of $\varepsilon(\mathbf{r})$ does not exist at the internal boundary $\partial\mathbb{P}$, Eqs. (7) must be supplemented with appropriate boundary conditions on the stochastic internal boundary $\partial\mathbb{P}$. Continuity of normal components of the electric displacement $\mathbf{D}(\mathbf{r})$ requires

$$\mathbf{n} \cdot \mathbf{D}(\mathbf{r})[\chi_{\mathbb{P}}(\mathbf{r}) - \chi_{\mathbb{M}}(\mathbf{r})] = 0, \quad \mathbf{r} \in \partial\mathbb{P} \tag{12}$$

and continuity of tangential components of the electric field $\mathbf{E}(\mathbf{r})$ requires

$$\mathbf{n} \times \mathbf{E}(\mathbf{r})[\chi_{\mathbb{P}}(\mathbf{r}) - \chi_{\mathbb{M}}(\mathbf{r})] = 0, \quad \mathbf{r} \in \partial\mathbb{P}\,, \tag{13}$$

where subscripts designate the fields in the regions $\mathbb{P}$ and $\mathbb{M}$, respectively, and $\mathbf{n}$ is the unit normal to the surface $\partial\mathbb{P}$. For the external boundary at the surface $\partial\mathbb{S}$, a variety of boundary conditions can be prescribed. The most common one is to specify

the values of $U(\mathbf{r})$ and/or the normal component of $\mathbf{D}(\mathbf{r})$ at the surface. When the composite medium and the boundary conditions are macroscopically uniform, the effective permittivity $\bar{\varepsilon}$ is independent of the precise nature of the macroscopic boundary conditions. Consequently, the particular choice of boundary conditions used in solving for $U(\mathbf{r})$ does not affect the value of $\bar{\varepsilon}$ obtained from Eq. (10). We solve the stochastic boundary value problem defined by Eqs. (7)–(9), (12) and (13) for $\mathbf{D}(\mathbf{r})$ and $\mathbf{E}(\mathbf{r})$ and then calculate the effective $\bar{\varepsilon}$ from Eq. (10).

4. Mean field mixing laws

Some of the widely used classical formulae for the effective permittivity of two component systems are summarised in Table 1. These mixing-laws are functions of the volume fraction and dielectric constant of each component. Except for the last formula (Lichtenecker) [12,13], the assumption is that a two-phase medium can be modelled as spherical grains embedded into a homogeneous background material (for details see [1,13,22,31,32]). An alternate mixing-law, the local porosity theory (LPT) was recently proposed [1,3,28,33]. It includes additional microstructure information through the geometric functions $\mu(\phi, L)$ and $\lambda(\phi, L)$. A brief derivation of this mixing law is presented next.

Consider a partitioning of the heterogeneous medium into n cubic cells $(\mathbb{K}_1, \ldots, \mathbb{K}_n)$ of side length L. Let

$$\mathbf{E}_{\mathbb{S}}(\mathbf{r}) = \mathbf{E}(\mathbf{r})\chi_{\mathbb{K}_1}(\mathbf{r}) + \cdots + \mathbf{E}(\mathbf{r})\chi_{\mathbb{K}_n}(\mathbf{r}) \,. \tag{14}$$

denote the exact solution for the electric field of the sample $\mathbb{S}$. The volume average of the electric field $\langle \mathbf{E}(\mathbf{r}) \rangle_{\mathbb{S}}$ is then calculated as

$$\begin{aligned} \langle \mathbf{E}(\mathbf{r}) \rangle_{\mathbb{S}} &= \frac{1}{V(\mathbb{S})} \left[\int_{\mathbb{K}_1} \mathbf{E}(\mathbf{r})\, \mathrm{d}\mathbf{r} + \cdots + \int_{\mathbb{K}_n} \mathbf{E}(\mathbf{r})\, \mathrm{d}\mathbf{r} \right] \\ &= \frac{1}{V(\mathbb{S})} \sum_{i=1}^{n} V(\mathbb{K}_i) \langle \mathbf{E} \rangle_{\mathbb{K}_i}(\mathbb{P}_i) \,, \end{aligned} \tag{15}$$

where $\langle \mathbf{E} \rangle_{\mathbb{K}_i}(\mathbb{P}_i)$ is defined as the volume average of the electric field in the ith cell $\mathbb{K}_i$. The argument $\mathbb{P}_i$ reminds us that the average depends upon the pore-space configuration inside the cell. Since the exact geometric description of the pore-space is generally unknown, it is rarely possible to solve the boundary value problem exactly and compute the average electric field $\langle \mathbf{E} \rangle_{\mathbb{K}_i}(\mathbb{P}_i)$. An approximate computation can still be made with the following assumptions.

The porous medium is assumed to be *spatially and statistically homogeneous*. Therefore, the average electric field $\langle \mathbf{E} \rangle_{\mathbb{K}_i}(\mathbb{P}_i)$ does not depend on the position of the cell $\mathbb{K}_i$ in the porous medium. Hence, $\langle \mathbf{E} \rangle_{\mathbb{K}_i}(\mathbb{P}_i) \approx \bar{\mathbf{E}}(L; \mathbb{P}_i)$ if all cells have the same shape $\mathbb{K}_i = \mathbb{K}$ and if this cell is sufficiently characterized by the size L. Neglecting the correlation between cells, we further assume that the pore-space configurations $\mathbb{P}_i$ in each cell are statistically independent. This condition will be approximately fulfilled for $L > \xi$ where the correlation length ξ is defined as the length at which the correlation

Table 1
Existing mean field theories (mixing laws) chosen for comparison with LPT

Inclusion shape	Mixing formula	Methods, references
Spheres	$\bar{\phi}\frac{\varepsilon_{\mathbb{P}}-\varepsilon_{eff}}{\varepsilon_{\mathbb{P}}+2\varepsilon_{eff}}+(1-\bar{\phi})\frac{\varepsilon_{\mathbb{M}}-\varepsilon_{eff}}{\varepsilon_{\mathbb{M}}+2\varepsilon_{eff}}=0$	EMA [11]
Spheres	$\bar{\varepsilon}=\varepsilon_{\mathbb{M}}\left(\frac{2\varepsilon_{\mathbb{M}}+\varepsilon_{\mathbb{P}}+2\bar{\phi}(\varepsilon_{\mathbb{P}}-\varepsilon_{\mathbb{M}})}{2\varepsilon_{\mathbb{M}}+\varepsilon_{\mathbb{P}}-\bar{\phi}(\varepsilon_{\mathbb{P}}-\varepsilon_{\mathbb{M}})}\right)$	Clausius–Mossotti (CMM) Host phase $\mathbb{M}$ [22,40]
Spheres	$\bar{\varepsilon}=\varepsilon_{\mathbb{P}}\left(\frac{3\varepsilon_{\mathbb{M}}+2\bar{\phi}(\varepsilon_{\mathbb{P}}-\varepsilon_{\mathbb{M}})}{3\varepsilon_{\mathbb{P}}-\bar{\phi}(\varepsilon_{\mathbb{P}}-\varepsilon_{\mathbb{M}})}\right)$	Clausius–Mossotti (CMP) Host phase $\mathbb{P}$ [22,40]
Spheres	$\bar{\varepsilon}^{1/3}=\bar{\phi}\varepsilon_{\mathbb{P}}^{1/3}+(1-\bar{\phi})\varepsilon_{\mathbb{M}}^{1/3}$	Looyenga (Loo) [14]
Spheres	$\frac{\bar{\varepsilon}-\varepsilon_{\mathbb{M}}}{\varepsilon_{\mathbb{P}}-\varepsilon_{\mathbb{M}}}\left(\frac{\varepsilon_{\mathbb{P}}}{\bar{\varepsilon}}\right)^{1/3}=\bar{\phi}$	Differential effective Medium (DEM) [41]
Arbitrary	$ln\bar{\varepsilon}=\bar{\phi}ln\varepsilon_{\mathbb{P}}+(1-\bar{\phi})\ln\varepsilon_{\mathbb{M}}$	Lichtenecker (Lic) [12]

function decays to $1/e$. The correlation function for a homogeneous medium is defined as

$$G(\mathbf{r}_0,\mathbf{r})=G(\mathbf{r}-\mathbf{r}_0)=\frac{\langle\chi_{\mathbb{P}}(\mathbf{r}_0)\chi_{\mathbb{P}}(\mathbf{r})\rangle-\langle\phi\rangle^2}{\langle\phi\rangle(1-\langle\phi\rangle)}\,. \tag{16}$$

For an isotropic medium $G(\mathbf{r})=G(|\mathbf{r}|)=G(r)$ with $G(0)=1$ and $G(\infty)=0$.

The second assumption is *local simplicity* [3]. It assumes that the local pore-space geometry $\mathbb{P}_i$ can be approximated by only a few numbers such as local porosity ϕ_i and the indicator function for the connectivity of the ith cell Λ_i, i.e., $\bar{\mathbf{E}}(L;\mathbb{P}_i)=\bar{\mathbf{E}}(L;\phi_i,\Lambda_i)$. The indicator function Λ is an essential geometric quantity for conductivity problems of porous media. It specifies whether a cell is conducting ($\Lambda=1$) or blocking ($\Lambda=0$).

Due to the above assumption, the spherical coated inclusion can now be used as a first approximation of the pore-space and matrix-space in each cell. We can then solve the boundary-value problem exactly and obtain the average electric field $\bar{\mathbf{E}}(L;\phi,\Lambda)$ for each cell. If $n=V(\mathbb{S})/V(\mathbb{K})$ is the number of cells in the partitioning of $\mathbb{S}$, Eq. (15) reduces to

$$\langle\mathbf{E}(\mathbf{r})\rangle\approx\frac{1}{n}\sum_{i=1}^{n}\bar{\mathbf{E}}(L;\phi_i,\Lambda_i)\,. \tag{17}$$

For each cell consider two concentrical spheres with a central sphere of dielectric constant ε_2 and a spherical shell of dielectric constant ε_1 embedded in a reference homogeneous medium with permittivity ε_0. This coated spherical inclusion is subjected to a constant electric field $\mathbf{E}_0=E_0\mathbf{e}_z$ (in positive z-direction). Using expansions into spherical harmonics and demanding continuity of tangential components of $\mathbf{E}(\mathbf{r})$ and normal components of $\mathbf{D}(\mathbf{r})$ at $|\mathbf{r}|=r=r_1$ (the radius of the shell) and $|\mathbf{r}|=r=r_2$ (the

radius of the core), along with the condition that $\mathbf{E} \to E_0$ as $r \to \infty$, one obtains the following solution for the electric field $\mathbf{E}$ (in cartesian coordinates $\mathbf{r} = (x, y, z)^{\mathrm{T}}$)

$$\mathbf{E}(x,y,z) = 3C_1 \frac{r_2^3}{r^5} z(x\mathbf{e}_x + y\mathbf{e}_y + z\mathbf{e}_z) - \left(C_2 + \frac{r_2^3}{r^3} C_1\right)\mathbf{e}_z \quad r_2 \leqslant |\mathbf{r}| \leqslant r_1 \,, \tag{18a}$$

$$= -C_3\mathbf{e}_z, \quad 0 \leqslant |\mathbf{r}| \leqslant r_2 \,, \tag{18b}$$

where $r^2 = x^2 + y^2 + z^2$. The coefficients in Eq. (18) are given by

$$C_i = \frac{3E_0\varepsilon_0\gamma_i}{(\varepsilon_1 + 2\varepsilon_0)(\varepsilon_2 + 2\varepsilon_1) + 2\eta(\varepsilon_1 - \varepsilon_0)(\varepsilon_2 - \varepsilon_1)} \,, \tag{19}$$

where $\gamma_1 = (\varepsilon_2 - \varepsilon_1)$, $\gamma_2 = -(\varepsilon_2 + 2\varepsilon_1)$, $\gamma_3 = -3\varepsilon_1$ and $\eta = (r_2/r_1)^3$.

Applying the effective medium approximation (EMA) or self-consistency approximation [1,17,23,34,35], we now take the effective medium with effective permittivity $\bar{\varepsilon}$ as the reference medium. As a result the volume average of the electric field in the inclusion (the concentric spheres) becomes equal to the average electric field in the whole body. Choosing spherical polar coordinates, substituting $\varepsilon_0 = \bar{\varepsilon}$ and then evaluating the integral of the electric field $\mathbf{E}$ over the volume of the coated spheres, we obtain the average electric field $\bar{\mathbf{E}}(L;\phi,\Lambda)$ of a cell $\mathbb{K}$ with porosity ϕ and connectivity Λ as

$$\bar{\mathbf{E}}(L;\phi,\Lambda) = 3E_0\bar{\varepsilon}\frac{(\varepsilon_2 + 2\varepsilon_1) + \eta(\varepsilon_1 - \varepsilon_2)}{(\varepsilon_1 + 2\bar{\varepsilon})(\varepsilon_2 + 2\varepsilon_1) + 2\eta(\varepsilon_1 - \bar{\varepsilon})(\varepsilon_2 - \varepsilon_1)}\mathbf{e}_z \,, \tag{20}$$

with $\eta = \Lambda(1-\phi) + (1-\Lambda)\phi$, $\varepsilon_1 = \Lambda\varepsilon_{\mathbb{P}} + (1-\Lambda)\varepsilon_{\mathbb{M}}$ and $\varepsilon_2 = \Lambda\varepsilon_{\mathbb{M}} + (1-\Lambda)\varepsilon_{\mathbb{P}}$. For percolating cells ($\Lambda = 1$) the core is made up of matrix material and the shell is made up of pore material. Thus, from Eq. (20) one can obtain $\bar{\mathbf{E}}(L;\phi,\Lambda=1)$ by substituting $\varepsilon_1 = \varepsilon_{\mathbb{P}}$, $\varepsilon_2 = \varepsilon_{\mathbb{M}}$ and $\eta = 1 - \phi$. For nonpercolating cells ($\Lambda = 0$) the interior-core is pore material and the shell is matrix material. Thereby, one replaces $\varepsilon_1 = \varepsilon_{\mathbb{M}}$, $\varepsilon_2 = \varepsilon_{\mathbb{P}}$ and $\eta = \phi$ in Eq. (20) to obtain $\bar{\mathbf{E}}(L;\phi,\Lambda=0)$.

In a real porous medium ϕ and Λ fluctuate from one cell to the next. Within LPT, these fluctuations are captured by $\mu(\phi)$ and $\lambda(\phi)$, respectively, and in the $\lim n \to \infty$, the sum in Eq. (17) becomes an integral

$$\langle \mathbf{E}(\mathbf{r}) \rangle \approx \int_0^1 \mu(\phi,L)\{\lambda(\phi,L)\bar{\mathbf{E}}(L;\phi,\Lambda=1) + [1-\lambda(\phi,L)]\bar{\mathbf{E}}(L;\phi,\Lambda=0)\}\,\mathrm{d}\phi \,. \tag{21}$$

Following a similar procedure we obtain an analogous expression for the average electric displacement

$$\bar{\mathbf{D}}(L;\phi,\Lambda) = 3E_0\bar{\varepsilon}\frac{\varepsilon_1[(\varepsilon_2 + 2\varepsilon_1) + 2\eta(\varepsilon_2 - \varepsilon_1)]}{(\varepsilon_1 + 2\bar{\varepsilon})(\varepsilon_2 + 2\varepsilon_1) + 2\eta(\varepsilon_1 - \bar{\varepsilon})(\varepsilon_2 - \varepsilon_1)}\mathbf{e}_z \,. \tag{22}$$

The derivation of expressions for percolating cells $\bar{\mathbf{D}}(L;\phi,\Lambda=1)$ and nonpercolating cells $\bar{\mathbf{D}}(L;\phi,\Lambda=0)$ is straightforward and an analogous equation of Eq. (21) for

$\langle \mathbf{D}(\mathbf{r}) \rangle$ can be obtained. Substituting this and Eq. (21) in Eq. (10) we obtain (after some algebraic simplification) the following mixing-law of LPT [1,27]:

$$\int_0^1 \mu(\phi, L)\lambda(\phi, L)\frac{\varepsilon_{CS}(\varepsilon_{\mathbb{P}}, \varepsilon_{\mathbb{M}}; 1-\phi) - \varepsilon_{LPT}}{\varepsilon_{CS}(\varepsilon_{\mathbb{P}}, \varepsilon_{\mathbb{M}}; 1-\phi) + 2\varepsilon_{LPT}}\,\mathrm{d}\phi + \int_0^1 \mu(\phi, L)[1-\lambda(\phi, L)]\frac{\varepsilon_{CS}(\varepsilon_{\mathbb{M}}, \varepsilon_{\mathbb{P}}; \phi) - \varepsilon_{LPT}}{\varepsilon_{CS}(\varepsilon_{\mathbb{M}}, \varepsilon_{\mathbb{P}}; \phi) + 2\varepsilon_{LPT}}\,\mathrm{d}\phi = 0\,, \tag{23}$$

where

$$\varepsilon_{CS}(\varepsilon_{\mathbb{P}}, \varepsilon_{\mathbb{M}}; 1-\phi) = \varepsilon_{\mathbb{P}}\left[\frac{3\varepsilon_{\mathbb{M}} + 2\phi(\varepsilon_{\mathbb{P}} - \varepsilon_{\mathbb{M}})}{3\varepsilon_{\mathbb{P}} - \phi(\varepsilon_{\mathbb{P}} - \varepsilon_{\mathbb{M}})}\right]\,. \tag{24}$$

Eq. (23) is solved numerically using a method combining bisection and inverse quadratic interpolation. For details see [36].

5. Length scales and limits of validity

For a given random medium $\mu(\phi, L)$ and $\lambda(\phi, L)$ can be measured experimentally (or numerically). Therefore, the solution of the mixing formula Eq. (23) provides a family of length scale dependent estimates $\varepsilon_{LPT}(L)$. Eq. (23), being a generalization of the effective medium approximation (EMA), is not valid in either the $\lim L \to 0$ when local geometries become strongly correlated or for $L \to \infty$ when the local simplicity assumption fails. The estimated effective permittivities are, therefore, expected to be valid only over an intermediate range of L.

In earlier works on LPT, various length scales relevant to the transport properties [1,27,28,37] have been studied. Although, some of the geometrical lengths like the correlation length or the largest grain size are found useful at times, they apparently have no direct link with connectivity of the microstructure. We introduce below three basic length scales associated with $p(L)$. Keeping in mind the range of validity of the EMA, we set the relevant intermediate length scale over which the estimates from LPT could be tested against estimates from other mixing formulae and exact calculations.

The threshold length L_c is defined by

$$p(L_c) = p_c\,, \tag{25}$$

where p_c is the percolation threshold. Although, the measurement cells are simple cubic lattices with $p_c = 0.3116$ (three-dimensional site percolation), within EMA $p_c = \frac{1}{3}$. Because $\varepsilon_{LPT}(L \leqslant L_c) = 0$ the threshold length L_c can be treated as a lower bound of the intermediate length scales. Note however, that L_c may not exist for samples with porosity $\bar{\phi} > p_c$ because $\lim_{L\to 0} p(L) = \bar{\phi}$.

In such situations, other physical length scales such as the two point correlation length ξ can be chosen as the lower bound. At this length scale the local geometries must be uncorrelated for the EMA to be valid.

The saturation length L_δ is defined as the length at which $p(L)$ approaches its asymptotic value $p(\infty)$ to a given degree of accuracy δ. For a percolating sample

$p(\infty) = 1$ and for a nonpercolating sample $p(\infty) = 0$. L_δ is defined through

$$L_\delta = \sup\{L : |p(\infty) - p(L)| \leqslant \delta\} \tag{26}$$

for small enough $\delta > 0$. The length L_δ may be equated with the size of the so called "representative elementary volume" (REV) [38] required for representativity with respect to connectivity. L_δ represents the size of an averaging (smoothing) region that is needed to ensure that the fluctuating microscopic connectivity can be replaced with an averaged connectivity field defined on the continuum. The small parameter δ controls the degree of smoothness and for sufficiently small δ, L_δ can be treated as an upper bound of the relevant intermediate range of lengths.

Finally, a percolation length L_p is defined from $p(L)$ through

$$\left.\frac{\mathrm{d}^2 p}{\mathrm{d}L^2}\right|_{L=L_p} = 0\,. \tag{27}$$

Hence L_p is the length around which $p(L)$, which is often sigmoidal in shape, changes most rapidly from its trivial value $p(0)=\bar{\phi}$ at small L to its other trivial value $p(\infty)=1$ at large L (here the porous medium is assumed globally connected). Geometrically, the length L_p marks the crossover from local to global connectivity. Note that $L_c < L_p < L_\delta$ for small enough δ and in the intermediate range of lengths the best validity of the underlying EMA within LPT is expected around this length scale.

6. Exact calculation of effective permittivities

The geometrical details of our samples are known within the limits of experimental resolution. Hence, the Laplace equation with variable permittivity $\varepsilon(\mathbf{r})$:

$$\nabla \cdot \varepsilon(\mathbf{r}) \nabla U(\mathbf{r}) = 0 \tag{28}$$

was solved directly for the discretized pore-space of the sandstones. Mixed boundary conditions were chosen such that a potential gradient is applied across the sample and the fluxes are set to zero on the other faces of the sample ($\partial U/\partial \mathbf{n} = 0$).

For the equivalent homogeneous effective medium, the effective permittivity ε_{ex} is determined through the relation:

$$\varepsilon_{ex} = \frac{D/A}{(U_b - U_a)/l} = \frac{D \cdot l/V}{(U_b - U_a)/l}\,. \tag{29}$$

Here $D = \int_{\mathbb{A}} \varepsilon \cdot \nabla U \, \mathrm{d}^2\mathbf{r}$ is the total electric displacement across the cross-section A and $(U_b - U_a)/l$ is the potential gradient applied between two opposite faces separated by a distance l. In a homogeneous medium the numerator and the denominator in Eq. (29) are equal to $\langle \mathbf{D}(\mathbf{r}) \rangle$ and $\langle \mathbf{E}(\mathbf{r}) \rangle$, respectively. Thus Eq. (29) is equivalent to Eq. (10).

A control-volume formulation [24,25] is used to discretize and solve Eq. (28) numerically. This ensures the conservation law Eq. (28) at both the local level (for each control volume) and the global level (for the whole solution domain). In order to

maintain the conservation of the fluxes the sample is subdivided into a number of nonoverlapping control volumes each of length a (the resolution) to ensure that there is one control volume surrounding each grid point i. As the starting point we use the integral form of the Laplace equation Eq. (28) over the control volume

$$\int_{\mathbf{V}} \nabla \cdot \varepsilon(\mathbf{r}) \nabla U(\mathbf{r}) \, \mathrm{d}\mathbf{r} = 0 \tag{30}$$

and transform the volume-integral into the surface-integral by using Gauss' divergence theorem

$$\int_{\mathbb{S}} (\varepsilon \nabla U) \cdot \mathbf{n} \, \mathrm{d}^2\mathbf{r} = 0 \,, \tag{31}$$

where $\mathbf{n}$ is the outward unit vector on the control-volume interface. In a three-dimensional cartesian coordinate system, $\nabla U \cdot \mathbf{n}$ is approximated in terms of the nodal (control-volume center) values:

$$\nabla U \cdot \mathbf{n} \approx \frac{(U_j - U_i)}{a} \,. \tag{32}$$

The net flux $(\varepsilon \nabla U) \cdot \mathbf{n}$ through the control volume boundary is the sum of the integrals over the six control volume faces. Eq. (31) reduces to

$$\sum_j \varepsilon_{ij} (U_j - U_i) a = 0 \,, \tag{33}$$

$$\varepsilon_{ij} = \frac{2\varepsilon_i \varepsilon_j}{\varepsilon_i + \varepsilon_j} \,, \tag{34}$$

where U_i is the electric potential at grid point i. The permittivity ε_{ij} on the surface of the volume element is approximated as the harmonic mean of permittivity ε_i and ε_j at grid points i and j, respectively. This approximation gives the correct result for the case $\varepsilon_i = 0$ or $\varepsilon_j = 0$ implying that the flux at the face of an insulator vanishes, as it should. This system of linear equations Eq. (33) with the given boundary conditions can be solved by any appropriate solver. The results in this work were obtained by using a conjugate gradient method with Jacobi preconditioning [39].

7. Results and comparison with approximate calculation

Discretised models of four different sedimentary rocks [29,30] have been analysed in this work. The three-dimensional (digitized) pore-space representations of these rocks were obtained experimentally by computerized microtomography. The digitization represents the samples on a cubic lattice of voxels. Different properties and the experimentally measured permeability k of these sandstones are summarised in Table 2.

Using the formulae in Section 2 $p(L)$ is measured for the four samples and plotted against L (in units of a) in Fig. 1. It was argued in [30] and is confirmed here that $p(L)$ contains crucial information about connectivity that allows to predict electrical conductivity. For all the four samples $p(L)$ is sigmoidal in shape. Using the definitions

Table 2
Properties of samples (sandstones) studied

	$a(\mu m)$	$M_1 \times M_2 \times M_3$	$\bar{\phi}$	ξ	k	L_c	L_p	L_δ	L_e
A	10	$95 \times 128 \times 128$	0.3200	2.9	5.5D	4.5	10 ± 1	19.2	9.0
B	30	$73 \times 128 \times 128$	0.2470	2.9	20D	8.5	13 ± 1	27.5	12.6
C	10	$128 \times 128 \times 128$	0.1775	3.4	1.1D	13.6	17 ± 3	46.9	16.6
D	7.5	$300 \times 300 \times 299$	0.1355	4.5	1.3D	24.8	31 ± 3	59.6	28.7

Type of samples: (A) fine Sst6d, (B) coarse Sst20d, (C) Berea and (D) Fontainebleau, their resolution a, dimension $M_1 \times M_2 \times M_3$, bulk porosity $\bar{\phi}$, the correlation length ξ, the experimental permeabilities k, threshold length L_c, percolation length L_p, saturation length L_δ with $\delta = 0.025$ and the dynamic length L_e (see Eq. (35)) for the four sandstones analysed.

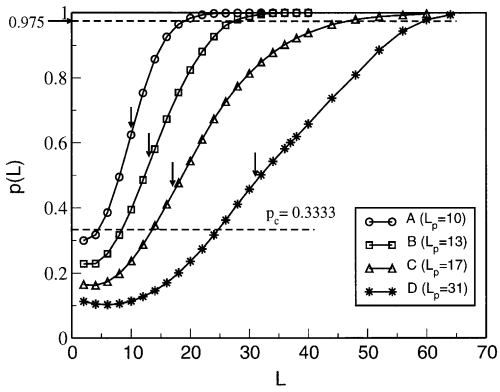

Fig. 1. Total fraction of percolating cells $p(L)$ of the four samples at different measurement cell sizes L (in the units of lattice constant). The upper dashed line corresponds to $p(L=\infty)-\delta = 0.975$. The lower dashed line is the percolation threshold for EMA. The arrows point at the percolation length L_p (given inside the legend in brackets for each sample).

presented in Section 5 we determine the threshold length L_c as the intersection point between $p(L)$ and $p_c = \frac{1}{3}$. The saturation length L_δ is obtained as the intersection point between $p(L)$ and the line $p(\infty) - \delta$ with $\delta = 0.025$. The percolation length L_p is obtained by numerically differentiating $p(L)$ (see Eq. (27)). The error in the evaluation of L_p depends on the smoothness of $p(L)$. The estimates of L_p along with estimates of the errorbars are presented in Table 2. For the samples analysed here, all these geometrical lengths L_c, L_δ and L_p depend inversely on the porosity $\bar{\phi}$ (see Table 2). However, this is not true in general. $p(L)$ can be very different for two samples with the same average porosities [30]. Such a sample with poor microscopic connectivity will have larger L_δ and L_p than one with good connectivity.

In Fig. 2 we have plotted $\varepsilon_{LPT}(L)$ obtained by solving (23) for infinite contrast, i.e., $\varepsilon_{\mathbb{P}}/\varepsilon_{\mathbb{M}} = \infty$. We have $\varepsilon_{LPT}(L < L_c) = 0$ and $\varepsilon_{LPT}(L > L_\delta)$ is nearly constant and much larger than the exact electrical permittivity ε_{ex} obtained by methods described in Section 6. For comparison purposes we introduce a dynamical length L_e defined

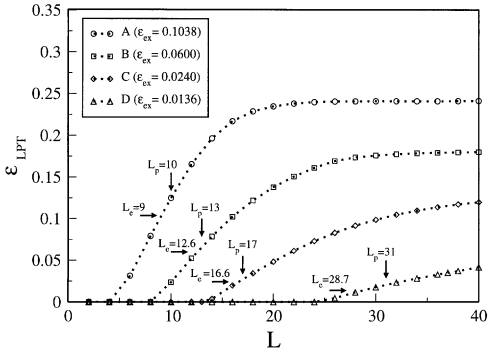

Fig. 2. LPT estimate of the electrical permittivity $\varepsilon_{LPT}(L)$ in the infinite contrast case for different sandstones. The corresponding numerically exact effective permittivity ε_{ex} (in brackets), L_e (horizontal arrow) and L_p (vertical arrow) are shown.

through

$$\varepsilon_{LPT}(L_e) = \varepsilon_{ex} \ . \tag{35}$$

L_e is thus the length at which the exact dielectric constant equals the approximate value obtained from LPT. The values for L_e for the four samples are also listed in Table 2. It is observed that L_e is close to L_p, and hence $\varepsilon_{LPT}(L_p)$ closely approximates ε_{ex} for these four sandstones.

By virtue of Eqs. (7)–(10), all effective permittivities $\bar{\varepsilon}$ depend on the contrast $\varepsilon_{\mathbb{P}}/\varepsilon_{\mathbb{M}}$. Therefore, L_e defined in Eq. (35) also depends on the ratio $\varepsilon_{\mathbb{P}}/\varepsilon_{\mathbb{M}}$. In the case of no contrast, $\varepsilon_{\mathbb{P}}/\varepsilon_{\mathbb{M}} = 1$, the curve $\varepsilon_{LPT}(L)$ is horizontal, i.e., $\varepsilon_{LPT}(L) = \varepsilon_{\mathbb{P}} = \varepsilon_{\mathbb{M}}$ for all L. For contrast close to this lowest value, the curves $\varepsilon_{LPT}(L)$ are so flat that it becomes numerically difficult to obtain a unique solution of Eq. (35). $\varepsilon_{LPT}(L)$ and ε_{ex} are measured for various values of contrast and L_e is estimated whenever unique solutions exist. In Fig. 3, these L_e are plotted against the ratio $\varepsilon_{\mathbb{P}}/\varepsilon_{\mathbb{M}}$ for all the four samples. It is seen that L_e is nearly constant and approaches the value for the infinite contrast. L_e is always lower than the percolation length L_p and seems to approach L_p for increasing contrast. For these four natural sandstones, the exact permittivities for five different contrasts, ranging from $\varepsilon_{\mathbb{P}}/\varepsilon_{\mathbb{M}} = 2.0$ to $\varepsilon_{\mathbb{P}}/\varepsilon_{\mathbb{M}} = \infty$, are summarized in Table 3 for future reference.

Table 4 presents the detailed comparison between the predictions of different mixing formulae and the exact values (ε_{ex}) for two choices of contrasts. For the case $\varepsilon_{\mathbb{P}}/\varepsilon_{\mathbb{M}} = 2.0$, all of the mixture laws including LPT provide comparably good results. But as the ratio $\varepsilon_{\mathbb{P}}/\varepsilon_{\mathbb{M}}$ is increased, the predictions from different mixture laws begin to differ significantly. Although the samples are fully connected, the effective permittivities calculated from EMA, CMM and Lic vanish in the limit of infinite contrast. The reason is that the average porosity of all the four samples are smaller than 1 for CMM and Lic and less than $\frac{1}{3}$ for EMA. Although CMP, Loo, DEM give finite effective permittivities, the predictions of LPT are in closer agreement with the *exact* results.

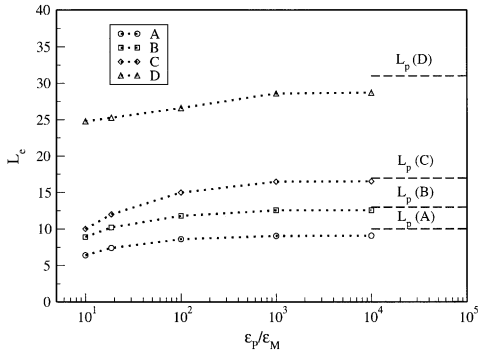

Fig. 3. The dynamical length L_e at which the LPT estimates match with the numerically exact results (see Section 6) for five different contrasts. The dashed line segments on the right indicate the value of L_p for the samples (in bracket).

Table 3
Numerically exact values (see Section 6) of the electrical permittivity $\bar{\varepsilon}$ at six different contrasts ($\varepsilon_{\mathbb{P}}/\varepsilon_{\mathbb{M}}$) for all four samples

$\varepsilon_{\mathbb{P}}/\varepsilon_{\mathbb{M}} \rightarrow$	2.0	10.0	18.6681	100.0	10000.0	∞
A	0.631896	0.252684	0.193043	0.124521	0.104032	0.103796
B	0.599673	0.207937	0.148954	0.081470	0.060319	0.060059
C	0.570113	0.169611	0.112065	0.046674	0.024353	0.024021
D	0.547499	0.147621	0.093615	0.034355	0.013924	0.013584

Table 4
Comparison of estimates of electrical permittivity $\bar{\varepsilon}$ from different mixing laws (Table 1) with the exact estimates (last row) for low contrast $\varepsilon_{\mathbb{P}}/\varepsilon_{\mathbb{M}} = 2.0$ and infinite contrast $\varepsilon_{\mathbb{P}}/\varepsilon_{\mathbb{M}} \rightarrow \infty$

	fine Sst6d (A)		coarse Sst20d (B)		Berea (C)		Fontainebleau (D)	
$\varepsilon_{\mathbb{P}}/\varepsilon_{\mathbb{M}}$	2.0	∞	2.0	∞	2.0	∞	2.0	∞
EMA	0.6342	0	0.6011	0	0.5710	0	0.5473	0
CMM	0.6304	0	0.5987	0	0.5697	0	0.5467	0
CMP	0.6408	0.2388	0.6073	0.1794	0.5762	0.1258	0.5514	0.0839
Loo	0.6354	0.0328	0.6026	0.0151	0.5724	0.0056	0.5486	0.0025
DEM	0.6377	0.1810	0.6044	0.1228	0.5737	0.0748	0.5557	0.0499
Lic	0.6242	0	0.5934	0	0.5655	0	0.5437	0
LPT	0.6387	0.1250	0.6037	0.0786	0.5761	0.0348	0.5472	0.0132
ex	0.6307	0.1038	0.5962	0.0600	0.5699	0.0240	0.5476	0.0136

Finally, we compare the results from different mixing-laws for varying contrast in more detail for the particular case of the Fontainebleau sample (D). In Fig. 4 we plot the effective permittivities as a function of the contrast for the Fontainebleau sandstone only. The values for infinite contrast are shown as horizontal line segments on the right. This is done for the exact effective permittivity and its approximations by mixing laws.

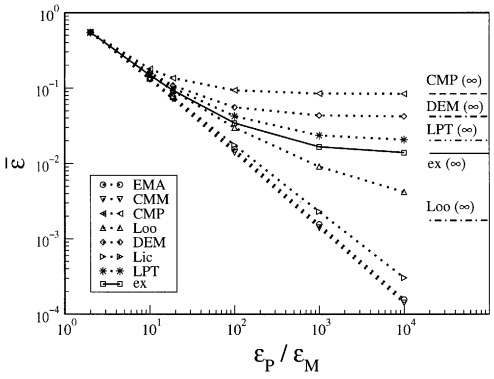

Fig. 4. The effective permittivity $\bar{\varepsilon}$ estimated for different contrasts for the Fontainebleau sandstone (D) from various mixing laws (abbreviations described in Table 1), LPT and exact value (ex). The horizontal line segments on the right correspond to the value of the effective permittivity $\bar{\varepsilon}$ at infinite contrast $\varepsilon_{\mathbb{P}}/\varepsilon_{\mathbb{M}} = \infty$ obtained from different mixing laws. The estimates from EMA, CMM and Lic vanish as $\varepsilon_{\mathbb{P}}/\varepsilon_{\mathbb{M}} \to \infty$.

The solid line with square symbols represents the exact result ε_{ex}. The LPT estimates for different values of the ratio $\varepsilon_{\mathbb{P}}/\varepsilon_{\mathbb{M}}$ are obtained at the percolation length $L_p = 31$. The LPT estimates give the closest approximation to the exact values over the full range of contrasts. Similar agreement is observed for the other three sandstones.

For the four samples available to us and analysed in this paper, LPT provides a reasonable estimate of the electrical permittivity at length L_p obtained from a purely geometrical function $p(L)$ that reflects quantitatively the microscopic connectivity at different length scales. This establishes that $\mu(\phi, L)$ and $\lambda(\phi, L)$ contain useful microscopic information that can lead to reasonable prediction of macroscopic transport parameters. This work corroborates the fact that a successful mixing theory must incorporate quantitative microscopic connectivity information. This conclusion is also important for geometric modelling of these media as found in [30]. The good agreement between LPT-estimates at L_p and the exact results suggests to extend the comparison to the case of hydrodynamic flow and effective fluid flow permeabilities.

Acknowledgements

We are grateful to the Deutsche Forschungsgemeinschaft and the Graduiertenkolleg “Modellierung und Diskretisierungsmethoden für Kontinua und Strömungen” for financial support.

References

[1] R. Hilfer, Adv. Chem. Phys. XCII (1996) 299.
[2] E. Hellen, M. Alava, K. Niskanen, J. Appl. Phys. 81 (1997) 6425.
[3] R. Hilfer, Phys. Rev. B 44 (1991) 60.

[4] M. Ioannidis, M. Kwiecien, I. Chatzis, Transp. Porous Media 29 (1997) 61.
[5] S. Roy, S. Tarafdar, Phys. Rev. B 55 (1997) 8038.
[6] C. Andraud, J. Lafait, A. Beghdadi, Phys. Rev. B 57 (1998) 13227.
[7] R. Pelster, Phys. Rev. B 59 (1999) 9214.
[8] A. Puzenko, N. Kozlovich, A. Gutina, Y. Feldmann, Phys. Rev. B 60 (1999) 14348.
[9] Clinton DeW, Van Siclen, Phys. Rev. E 59 (1999) 2804.
[10] J.S. Andrade, D.A. Street, Y. Shibusa, S. Havlin, H. Stanley, Phys. Rev. E 55 (1997) 772.
[11] D. Bruggeman, Ann. Phys. 24 (1935) 636.
[12] K. Lichtenecker, K. Rother, Phys. Z 32 (1931) 255.
[13] J. Reynolds, J. Hough, Proc. Phys. Soc. London 70 (1957) 769.
[14] H. Looyenga, Physica 31 (1965) 401.
[15] Z. Hashin, S. Shtrikman, J. Appl. Phys. 33 (1962) 3125.
[16] D. Bergman, Ann. Phys. 138 (1982) 78.
[17] M. Beran, Statistical Continuum Theories, Wiley, New York, 1968.
[18] R. Hilfer, in: D. Stoyan, K. Mecke (Eds.), Räumliche Statistik und Statistische Physik, Springer, Berlin, 2000.
[19] A. Tscheschel, D. Stoyan, R. Hilfer, Physica A, to be published.
[20] D. Stoyan, W. Kendall, J. Mecke, Stochastic Geometry and its Applications, Wiley, Chichester, 1987.
[21] C. Manwart, S. Torquato, R. Hilfer, Phys. Rev. E 62 (2000) 893.
[22] C. Böttcher, Theory of Electric Polarization, Vol. I, Elsevier, Amsterdam, 1973.
[23] P. Sheng, Introduction to Wave Scattering, Localization, and Mesoscopic Phenomena, Academic, San Diego, 1995.
[24] S. Patankar, Numerical Heat Transfer and Fluid Flow, Hemisphere, New York, 1980.
[25] J. van Kan, A. Segal, Numerik partieller. Differentialgleichungen für Ingenieure, B.G. Teubner, Stuttgart, 1995.
[26] D. Stauffer, A. Aharony, Introduction to Percolation Theory, Taylor & Francis, London, 1992.
[27] J. Widjajakusuma, B. Biswal, R. Hilfer, Comput. Mater. Sci. 16 (1999) 70.
[28] J. Widjajakusuma, C. Manwart, B. Biswal, R. Hilfer, Physica A 16 (1999) 70.
[29] B. Biswal, C. Manwart, R. Hilfer, Physica A 225 (1998) 221.
[30] B. Biswal, C. Manwart, R. Hilfer, S. Bakke, P. Øren, Physica A 273 (1999) 452.
[31] C. Böttcher, P. Bordewijk, Theory of Electric Polarization, Vol. II, Elsevier, Amsterdam, 1978.
[32] R. Landauer, in: J. Garland, D. Tanner (Eds.), Electrical Transport and Optical Properties of Inhomogeneous Materials, AIP, New York, 1978.
[33] R. Hilfer, Physica A 194 (1993) 406.
[34] E. Kröner, in: CISM Courses and Lectures No. 92, Udine, Springer, Wien, 1972.
[35] E. Kerner, Proc. Phys. Soc. London, Sect. B 69 (1956) 802.
[36] W. Press, S. Teukolsky, W. Vetterling, B. Flannery, Numerical Recipes in Fortran. The Art of Scientific Computing, 2nd Edition, Cambridge University Press, Cambridge, 1992.
[37] F. Boger, J. Feder, R. Hilfer, T. Jøssang, Physica A 187 (1992) 55.
[38] J. Bear, Dynamics of Fluids in Porous Media, Elsevier, New York, 1972.
[39] R. Barrett, et al., Templates for the Solution of Linear Systems: Building Blocks for Iterative Methods, SIAM, Philadelphia, 1994.
[40] J. Maxwell, A Treatise on Electricity and Magnetism, Vols. 1,2, Dover, New York, 1954.
[41] P. Sheng, Geophysics 56 (1991) 1236.